



Politecnico di Milano

Orbital Mechanics

Academic Year 2023/2024

Final Project Report

Interplanetary and Planetary Explorer Missions

Project group n. 2307

Team members:

Surname	Name	Matriculation number	Person code
Bellini	Davide	247658	10710744
Mensi Weingrill	Edoardo	244706	10706185
Mirri	Pietro	244858	10765536
Nuccio	Gabriele	247457	10730683

1. Interplanetary Explorer Mission

The PoliMi Space Agency is carrying out a feasibility study for a potential Interplanetary Explorer Mission visiting a body in the Solar System, with an intermediate flyby on a planet.

In this section of the report, we analyse an interplanetary transfer from Earth to Mercury with an intermediate flyby on Venus.

The requested mission presents the following constraints: first possible departure from Earth on the 1st January 2028 at 00:00, latest possible arrival on Mercury on the 1st January 2058 at 00:00.

1.1 Mission Overview

For mission design, the team has chosen to optimize the total cost in terms of velocity variation (ΔV_{tot}) starting from three temporal variables: the departure time (t_{dep}), the time of flight from Earth to Venus (ToF_1) and the time of flight from Venus to Mercury (ToF_2). The considered problem constraints are the latest possible arrival on Mercury (t_{max}) imposed by the mission specifications and the minimum distance from Venus of 500 km (r_{p_min}) to avoid the planet's dangerous atmosphere. To realize that the '*patched conics method*' was used.

The chosen mission design presents a preliminary analysis of the time windows, iterative research in a grid of possible outputs, then an optimization with a genetic algorithm of the best solutions followed by another run of the genetic algorithm in the neighborhood of the solution to find the final results, finally those results are presented and plotted.



1.2 Preliminary Analysis

Due to the impossibility of analyze every possible combination given by the problem variables, the team try to find a repeated pattern for the departure time and the optimal time of flights to go from Earth to Venus and from Venus to Mercury.

The synodic periods between Earth – Venus and Venus – Mercury are computed to try to find an optimal departure from Earth.

$$T_{Syn} = \frac{T_1 \cdot T_2}{|T_2 - T_1|}$$

The team has chosen to study the two Lambert's arcs for Earth-Venus and Venus-Mercury transfers within the feasible time interval for the mission. In this preliminary analysis each transfer is treated as an independent mission. To ensure acceptable computational time without losing too much precision, it was decided to span all possible departure and arrival dates with a step of 10 days. Therefore, it was possible to compute the Pork-Chop Plots of the two manoeuvres.

From the results we could notice that, in both cases, the needed velocity variation grows exponentially after the first time of flight lasts under 30 days or above 300 days and the second one lasts under 10 days or above 200 days, hence the admitted time of flights were restricted in the sequent range [50 days – 300 days] for Earth-Venus lambert arc and [20 days – 200 days] for Venus-Mercury lambert arc.

It was also possible to observe a repeated pattern in the Pork-Chop Plots every synodic period, so the team has chosen to consider a fixed number (20) of departures for each synodic period that guarantees around a departure per months in the whole window.

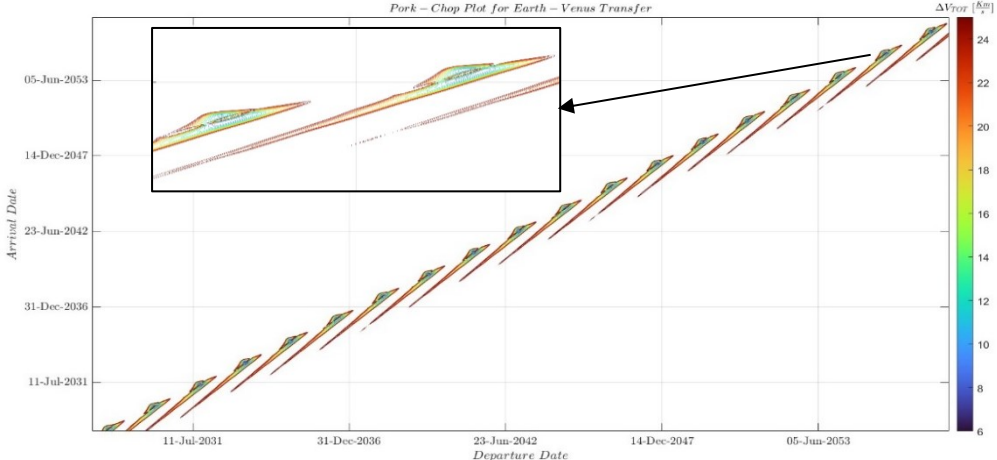


Figure 1.1: Earth-Venus Pork-chop plots, only ($\Delta V < 25$ levels)

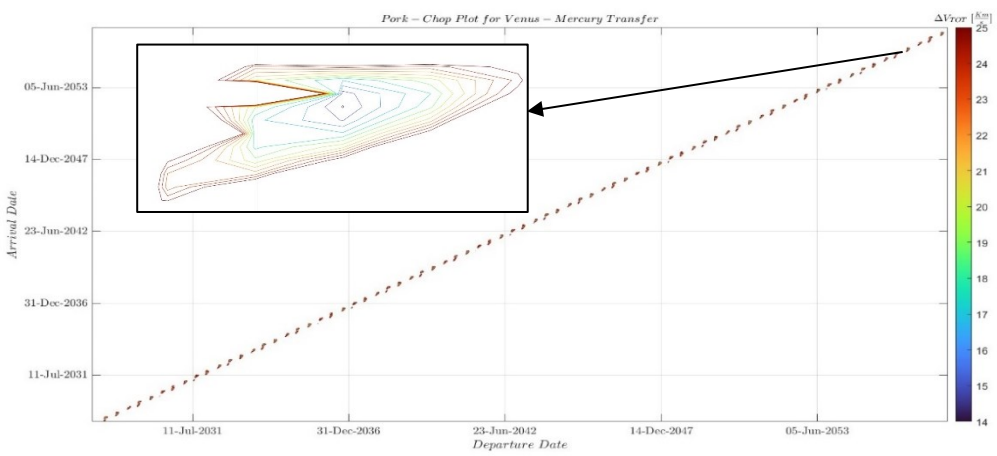


Figure 1.2: Venus-Mercury Pork-chop plots, only ($\Delta V < 25$ levels)

1.3 Grid Search

After the preliminary analysis, to obtain the first results for the mission, an iterative algorithm was implemented. The algorithm is composed of three “for” loop cycles, one for each variable of the problem (t_{dep} , ToF_1 , ToF_2) and create a 3D array containing all the possible ΔV_{tot} for the evaluated trajectories, if the flyby requests a pericentre radius minor than the minimum affordable r_{p_min} the function assign the NaN value to ΔV_{tot} , and so the option is excluded. Here is presented the program’s structure:

```

for each departure time
    get Earth Keplerian parameters and transform into Cartesian ones
    for each time of flight from Earth to Venus  $ToF_1$ 
        get Venus Keplerian parameters and transform into Cartesian ones
        compute the first Lambert Arc
        compute the velocity variation of the first manoeuvre
        for each time of flight from Venus to Mercury  $ToF_2$ 
            get Mercury Keplerian parameters and transform into Cartesian ones
            compute the second Lambert Arc
            compute the velocity variation of the second manoeuvre
            compute the flyby manoeuvre
            compute the sum of all the three manoeuvres
    end
end
end

```

At the end of this program a simple function called '*bestsolutions*' runs to find the five best ΔV_{tot} results in the grid

1.4 Genetic Algorithm

To proceed in the analysis the team has chosen to use a Genetic Algorithm, an algorithm based on the natural selection which starts from an initial solutions' population and evolve it with crossover and mutation functions, recreating each iteration a new population of optimal individuals since it converges to an optimal solution. The genetic algorithm does not guarantee a convergence to the global minimum of the problem when the initial conditions are not enough restrictive, hence the algorithm was run in the neighbourhoods of the solutions found in the Grid Search section.

To implement the algorithm, the '*ga*' function of MATLAB is used, the team created the function to optimized using the same functions presented in the grid search, this time obviously without the loop cycles. After the setting of the problem constraints also the options were defined to guarantee, once again, acceptable computational time without losing a good convergence of the algorithm.

The algorithm was run for each of the top five results from '*Grid Search*' function and then the optimal result was selected.

After the first run of '*ga*' we could observe that the mean value of the final population, is quite distance from the found minimum, so it was performed a second '*ga*' run, with even more stringent conditions in terms of time of flight in the neighbourhoods of the best solution, also the options were changed in order to obtain a non-integer result finding not only the days of the best solution but also hours, minutes and seconds. To get a final optimization in this run the options presents a minimizing Matlab function '*fmincon*' which runs when '*ga*' terminate.

1.5 Results and conclusions

The final solution is presented in this section: the mission will start on December 16th, 2056 at 16:50:58, the flyby will be performed on March 27th, 2057 at 2:49:07 and the spacecraft will arrive to Mercury on May 5th, 2057 at 12:30:50. Hence the first ToF_1 will be of 92 days, 11 hours, 28 minutes and ToF_2 of 48 days, 17 hours, 54 minutes.

DEPARTURE	FLYBY	ARRIVAL
December 16 th , 2056 16:50:58	March 27 th , 2057 2:49:07	May 5 th , 2057 12:30:50

Table 1.1: Mission dates

1.5.1 Heliocentric trajectory

Knowing the dates is possible to characterise the two heliocentric transfer arcs in Keplerian elements using the function (*uplanet*).

	a [km*10 ⁶]	e	i [deg]	Ω [deg]	ω [deg]	ϑ_{dep} [deg]	ϑ_{arr} [deg]
Earth	119.2042	0.2344	0.0530	94.0126	181.2509	178.7491	280.8750
Venus	86.9393	0.304	6.8345	41.8198	306.2516	207.9238	316.1506

Table 1.2 : Keplerian elements of heliocentric legs

1.5.2 Flyby (powered gravity assist)

When the spacecraft reaches Venus a flyby is performed at the closest approach to the planet, to take advantage of Venus gravity. To match the conditions of the velocities before and after the flyby a small,

powered manoeuvre is needed, and it will be performed at the common pericentre of the two hyperbolas $r_p = 6551.80 [km]$ which gives a little extra cost to the mission: $\Delta V_{ga} = 0.1057 [\frac{km}{s}]$.

The total manoeuvre gives an advantage in terms of velocity variation of $\Delta V_{fb} = 6.9562 [\frac{km}{s}]$ given by the norm of the difference between the two infinite velocities after the flyby $\Delta V_{fb} = ||v_\infty^+ - v_\infty^-||$, that is very significant compared to the manoeuvre cost: $\frac{\Delta V_{ga}}{\Delta V_{fb}} = 0.0152$, which represents only the 1.52% of the total gain.

Then, the permanence time inside the Venus' SOI has been computed using the hyperbolic time law, considering the time to go from the intersection between the first arc and the SOI till the intersection with the second arc. Once knowing θ_{SOI} , obtained through the Orbit Equation $(R_{SOI} = \frac{h^2}{\mu} \frac{1}{1+e \cos \theta_{SOI}})$ where $R_{SOI} = R_{Sun-Venus} \left(\frac{m_{Venus}}{m_{Sun}} \right)^{\frac{2}{5}}$, we have:

$$F_{SOI \rightarrow p} = 2 \operatorname{atanh} \left(\sqrt{\frac{e-1}{e+1}} \tan \frac{\theta}{2} \right) \xrightarrow[\text{Time Law}]{\text{Kepler's}} M_h = e \sinh(F_{SOI \rightarrow p}) - F_{SOI \rightarrow p} \implies t_{SOI \rightarrow p} = \frac{M_h}{\frac{\mu^2}{h^3} (e^2 - 1)^{\frac{3}{2}}}$$

$$t_{flyby} = 2 t_{SOI \rightarrow p} = 40 \text{ h } 16 \text{ m } 58 \text{ s.}$$

r_p [km]	t_{flyby} [h, m, s]	ΔV_{fb} [km/s]	ΔV_{ga} [km/s]
6551.80	[40, 16, 58]	6.9562	0.1057

Table 1.3: Fly-by outcomes

1.5.3 Cost of the mission in terms of ΔV_{tot}

In this section are presented the cost of each manoeuvre of the mission ΔV_{dep} , ΔV_{ga} , ΔV_{arr} which represent the cost of the first manoeuvre to leave Earth and enter in the first Heliocentric arc, the powered gravity assist manoeuvre discussed in the previous section and the final manoeuvre to reach Mercury.

It is also computed the optimal value of the total cost of the mission: $\Delta V_{tot} = \Delta V_{dep} + \Delta V_{ga} + \Delta V_{arr}$

ΔV_{dep} [km/s]	ΔV_{ga} [km/s]	ΔV_{arr} [km/s]	ΔV_{tot} [km/s]
4.2784	0.1057	8.2339	12.6180

Table 1.4: costs of the manoeuvres

1.5.4 Conclusions

We have chosen the solution imposing the only criteria of minimizing the total cost, without any constraints on the time windows because the total cost of the mission is still high for real applications after all the optimizations done.

We also noticed that our mission's departure is very far in time and the arrival is very close to the maximum acceptable arrive, so we want to propose an alternative solution, which present a slightly higher cost, but guarantees a departure and arrival time ten years earlier. The data of this possible choice are presented in the following table:

DEPARTURE	FLYBY	ARRIVAL	ΔV_{tot} [km/s]
December 2 nd , 2045 09:34:29	May 20 th , 2046 03:20:58	September 7 th , 2047 12:39:24	12.8776

Table 1.5: Alternative mission outcomes

We could observe an increment on the ΔV_{tot} of: 0.2596 [km/s], which is not very high respect to the total velocity needed but, once again, our goal was to find the most feasible mission and so we have chosen to pick the solution related to the lowest possible value of ΔV_{tot} .

1.6 Plots

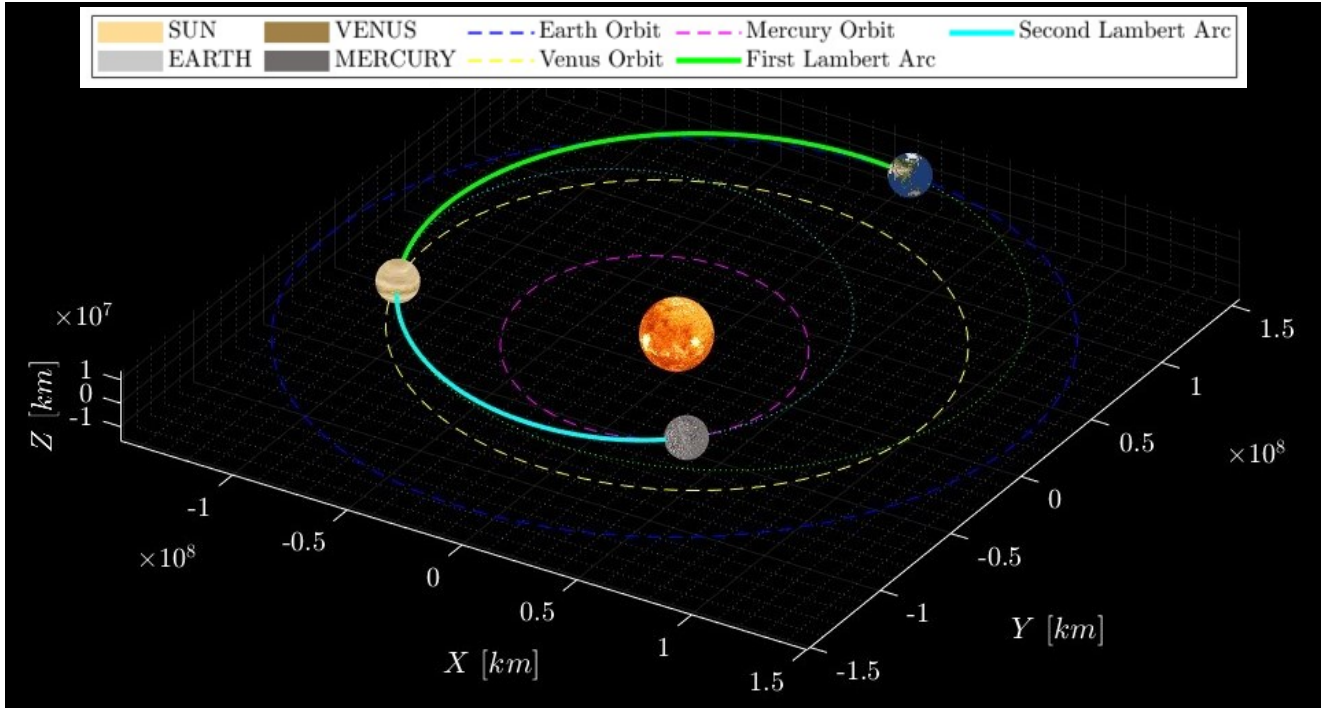


Figure 1.1: Interplanetary mission summary

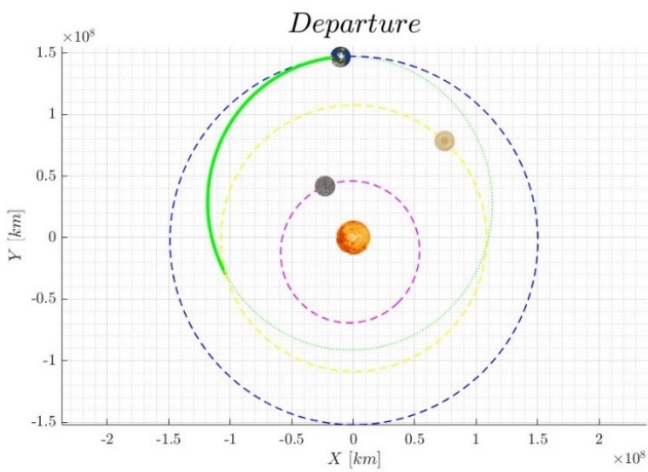


Figure 1.4.a) Departure from Earth

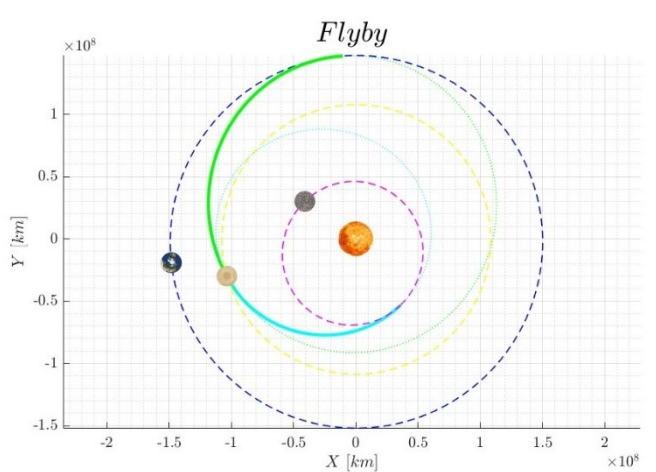


Figure 1.4.b) Fly-by at Venus

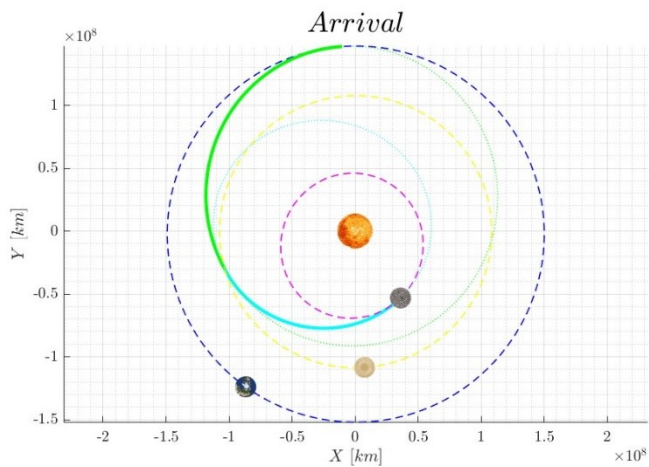


Figure 1.4.c) Arrival at Mercury

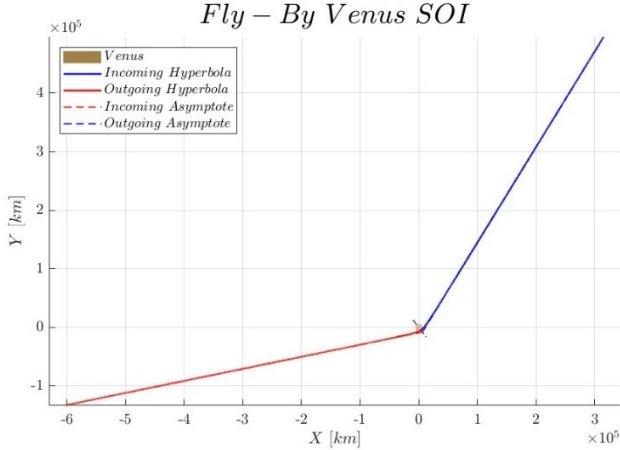


Figure 1.5: flyby on Venus (SOI field of view).

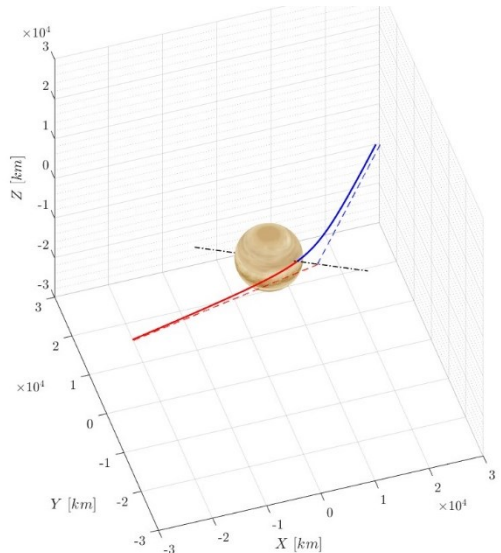


Figure 1.6: flyby on Venus. (Zoom on the planet).

2. Planetary Explorer Mission

The PoliMi Space Agency wants to launch a Planetary Explorer Mission, to perform Earth observation.

In this part of the report, we will analyse a LEO (Low-Earth Orbit) orbit and we will characterize the ground track. We will also propose an orbit modification to reach a repeating ground track. Then we will study the effect of orbit perturbations on the orbit assigned, both in terms of how does our ground track change and the variation of the orbital parameters. We will consider as perturbations the J2 effect and the Atmospheric Drag, and we will compare different propagation methods. We have also performed a filtering of high frequencies in the orbital parameters to retrieve the long period and/or secular evolution of the perturbations analysed. At the end, we have performed a comparison with real data, selecting a debris in the same orbital region and comparing the ephemeris with the orbit propagated with the model designed.

*Non esortare
LEO, basso pericentro
ma alto apocentro
LEO $\rightarrow h < 2000 \text{ Km}$*

2.1 Nominal Orbit Characterization

The initial Earth-centred orbit assigned is characterized by the following orbital parameters:

Table 2.1: Initial Orbital Elements

$a [\text{km}]$	$e [-]$	$i [\text{deg}]$	$\Omega [\text{deg}]$	$\omega [\text{deg}]$	$\theta [\text{deg}]$	T_{orbit}
17264	0.6098	49.257	0	0	0	6 h : 15 min : 15 s

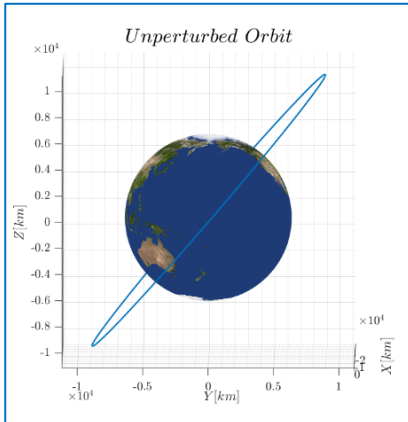


Figure 2.2: Spacecraft Orbit (y-z plane)

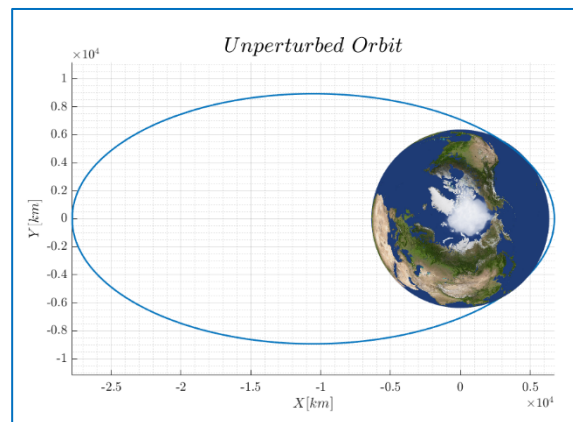


Figure 2.1: Spacecraft Orbit (x-y plane)

The last three parameters we decided to set them to zero, as we could decide them freely.

The perturbations considered in this assignment are:

- *J2 Effect* (i.e. the second zonal harmonic of Earth): Perturbation due to Earth's oblateness. The perturbing acceleration associated with is computed as:

$$\mathbf{a}_{J_2} = \frac{3}{2} \frac{J_2 \mu_E R^2}{r^5} \left[\left(5 \frac{z^2}{r^2} - 1 \right) x \hat{\mathbf{i}} + \left(5 \frac{z^2}{r^2} - 1 \right) y \hat{\mathbf{j}} + \left(5 \frac{z^2}{r^2} - 3 \right) z \hat{\mathbf{k}} \right] \quad (2.1)$$

where $J_2 = 0.00108263$

- *Atmospheric Drag*: Perturbation due to Earth's atmosphere (Negligible for altitude over 1000 Km). The perturbing acceleration associated with is calculated as:

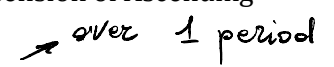
$$\mathbf{a}_{\text{drag}} = -\frac{1}{2} \rho v_{\text{rel}}^2 C_D A_m \frac{\mathbf{v}_{\text{rel}}}{\|\mathbf{v}_{\text{rel}}\|} \quad (2.2)$$

where ρ is the atmospheric density expressed in $\frac{Kg}{m^3}$ at the spacecraft altitude over the sea level, v_{rel} is the spacecraft relative velocity with respect to the atmosphere, C_D is the dimensionless drag coefficient and A_m is the cross-sectional area of the spacecraft per unit mass.

2.2 Ground Track

The ground track is the projection of the satellite's orbit onto the Earth's surface. At a given instant, we can imagine a radial line drawn outward from the centre of the Earth to our satellite. We locate the point where this imaginary line pierces the Earth's surface by giving its latitude ϕ and longitude λ relative to the Earth. As the satellite moves around Earth, the trace of these points is the ground track.

While the spacecraft moves along its orbit, we see that its ground track is subjected to a shift. This shift is mainly due to 2 factors:

- *Earth Rotation*: as Earth rotates eastward beneath the spacecraft orbit at 15.04 deg/h, the ground track will advance westward with the same rate.
- *J_2 Perturbation*: Earth's oblateness has a secular effect on the RAAN (Right Ascension of Ascending Node) Ω , on the Argument of Perigee ω and on the True Anomaly θ . 

Speaking about ground track, what we are interested in is the variation of the longitude $\Delta\lambda$ of the spacecraft's projection over the Earth' surface. The combination of the two effects is given by the formula:

$$\Delta\lambda_{tot} = \left[-\frac{2\pi T_{orbit}}{T_E} \right] + (\dot{\Omega}_{sec} + \dot{\omega}_{sec} + \dot{M}_{sec}) T_{orbit} \rightarrow$$

Force per gli
 retini due (2.3)
 tenimi va
 appunto qualcosa
 per far vedere che
 i due forze si
 su alte λ

$$\dot{\Omega}_{sec} = -\frac{3}{2} \frac{\sqrt{\mu_E} R_E^2 J_2}{(1-e^2)^2 a^2} \cos i$$

$$\dot{\omega}_{sec} = -\frac{3}{2} \frac{\sqrt{\mu_E} R_E^2 J_2}{(1-e^2)^2 a^2} \left(\frac{5}{2} \sin^2 i - 2 \right)$$

$$\dot{M}_{sec} = \frac{3}{2} \frac{\sqrt{\mu_E} R_E^2 J_2}{(1-e^2)^2 a^2} \left(1 - \frac{3}{2} \sin^2 i \right) \quad (2.6)$$

As can be noted, since we have a prograde orbit ($0^\circ < i < 90^\circ$), due to J_2 perturbation we have that:

- the secular effect on RAAN Ω is negative, hence the node line drifts westward. This phenomenon is called the Regression of the Nodes, as the RAAN will continuously decrease.
- the secular effect on Argument of Perigee ω is positive, hence the perigee advances in the direction of motion. This phenomenon is called Perigee Precession, which leads to an eastward drift of λ .
- the secular effect on Mean Anomaly M is positive, hence our satellite is moving along its orbit in the direction of motion, thus inducing again an eastward drift of λ .

While J_2 perturbation affects directly the RAAN, the principal effects of the Atmospheric Drag upon the orbit are to reduce its size (decreases the semi-major axis a) and to circularise it (decreases the eccentricity e). This doesn't mean that its perturbation can't be seen in the ground track. Indeed, as both a and e decrease, the second term in Eq. (2.3) will increase. Furthermore, since:

$$T_{orbit} = 2\pi \sqrt{\frac{a^3}{\mu}} \quad (2.7)$$

the orbital period decreases due to atmospheric drag, and consequently, as it can be seen in Eq. (2.3), also the term related to Earth's Rotation increases. In conclusion, both J_2 perturbation and Atmospheric Drag contribute to the variation of the longitude. In the following figures, the comparison is shown between the ground track of the spacecraft in both the unperturbed and perturbed cases, considering significant time intervals.

Figure 2.3: Ground track after 1 orbit

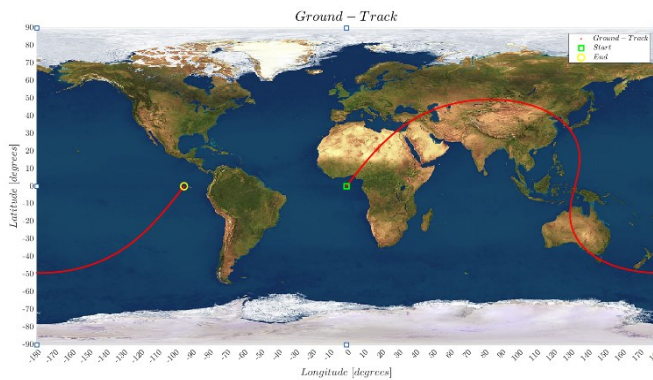


Figure 2.3.a): Unperturbed

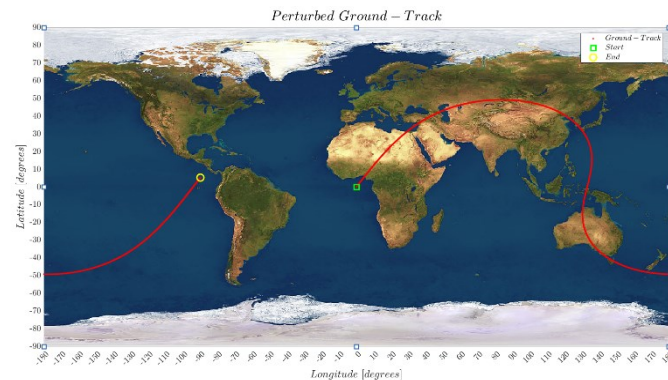


Figure 2.3.b) Perturbed

Figure 2.4: Ground Track after 1 day

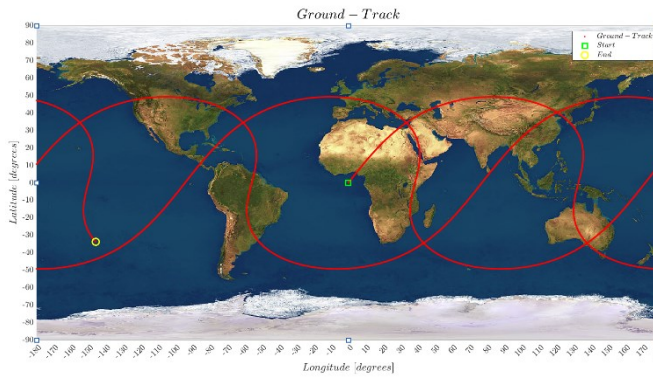


Figure 2.4.a) Unperturbed

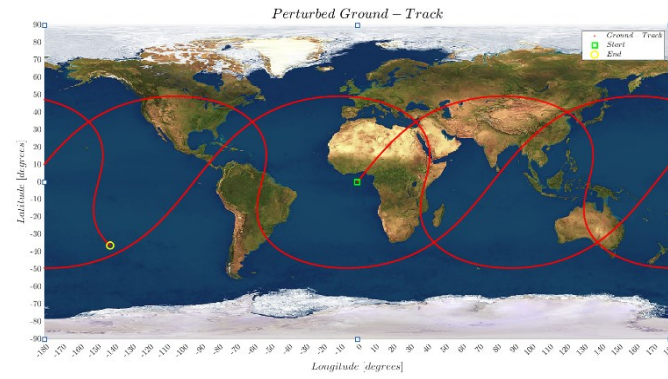


Figure 2.4.b) Perturbed

Figure 2.5: Ground Track after 5 days

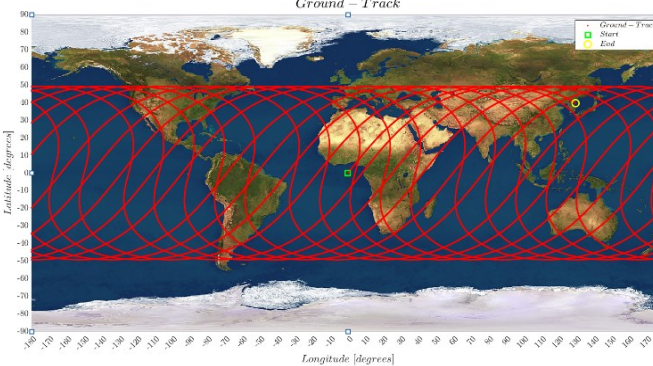


Figure 2.5. a) Unperturbed

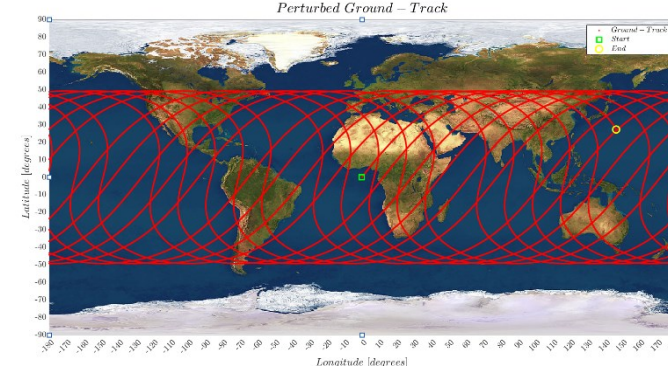


Figure 2.5. b) Perturbed

As we can see, the impact of the perturbation due to J_2 on the variation of longitude visible in the ground track is far less compared to that of Earth's Rotation. This occurs since, despite pericentre altitude being extremely low ($alt_p = 365.4 \text{ Km}$), the apocentre radius is significant ($r_a = 27792 \text{ Km}$). Indeed, due to the highly eccentric orbit and a rather elevated value of a , the effect of J_2 decreases as the spacecraft becomes farther from the bulge and its gravitational influence.

At the same time, it is very interesting to notice that the J_2 effect does not lead to a westward drift as it can be expected, but to an **eastward drift**. This occurs due to the combination of our orbital parameters (inclination i , eccentricity e and semi-major axis a), whereby the combined effect due to $\dot{\omega}_{sec}$ and \dot{M}_{sec} on the satellite's longitude λ (rotation towards East) exceed the one due to $\dot{\Omega}_{sec}$ (rotation towards West).

2.2.1 Repeating Ground Track

For the ground track to repeat periodically, i.e. for our satellite to return above the same location on the Earth's surface, the following condition must be satisfied:

$$k \Delta\lambda = m 2\pi \quad (2.8)$$

where k is the number of revolutions of the satellite and m the number of Earth's revolutions. Given the values of $k = 15$ and $m = 4$, we need to modify our initial orbit to obtain a repeating ground track. Since the effect of Earth's Rotation is far greater than the one due to J_2 , we can consider $\Delta\lambda$ as: $\Delta\lambda = \omega_E T_{orbit}$, where ω_E is the Earth's rotation velocity (15.04 deg/h). Substituting in Eq. 2.4 and operating, we can see that is equivalent to imposing that the ratio of the satellite's orbital period T_{orbit} and the Earth's rotational period $T_E = \frac{2\pi}{\omega_E}$ is a rational number:

$$\frac{T_{orbit}}{T_E} = \frac{m}{k} \rightarrow T_{orbit} = \frac{2\pi m}{\omega_E k} \quad (2.9)$$

From Eq. 2.9, and recalling Eq. 2.7, we obtain the value of semi-major axis a :

$$a = \sqrt[3]{\frac{\mu m^2}{\omega_E^2 k^2}} = 17469.344 \text{ Km} \quad (2.10)$$

Once obtained a of the modified orbit, while keeping the other orbital parameters unchanged, we can easily derive the ground track of the modified orbit, both in the unperturbed and perturbed cases, as shown in the following figures.

Figure 2.6: Repeating Ground track after 12 satellite's revolutions and 3 Earth's revolutions

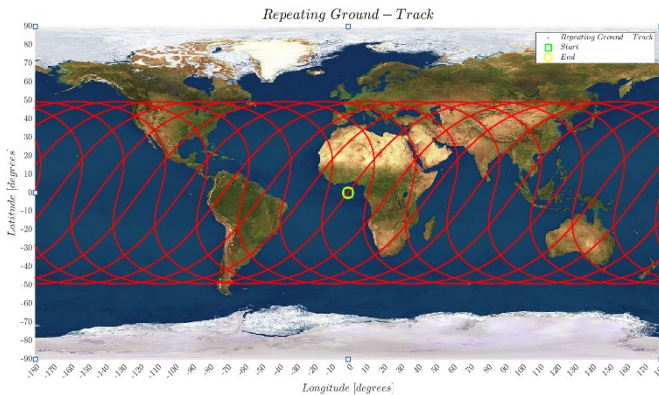


Figure 2.6.a) Unperturbed

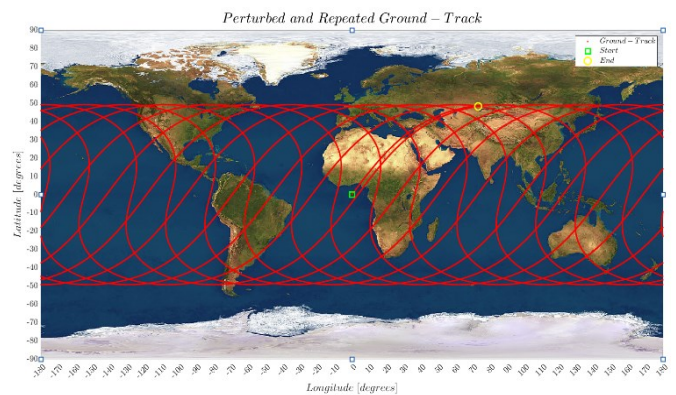


Figure 2.6.b) Perturbed

As it can be seen from the figures above, the exact repetition of the ground track occurs only when we are dealing with the unperturbed 2 Body Problem. Instead, when accounting the J_2 effect, we see that, even with a modified semi-major axis, the ground track doesn't repeat. This is strictly related to the nature of the perturbed 2 Body Problem. Indeed, the gravitational perturbation due to J_2 not only impacts the RAAN of our orbit ($\dot{\Omega} < 0$) leading to the regression of the nodal line, but it also leads to the precession of the Argument of Perigee ($\dot{\omega} > 0$), and the Mean Anomaly $\dot{M} > 0$. All these effects are not taken into account in Eq. 2.5, as it is indeed an approximation, and, as a consequence, the ground track, in the perturbed 2-body problem scenario, does not exhibit exact repetition.

2.3 Orbit Propagation

To propagate the initial orbit while accounting for both the J_2 effect and the Atmospheric Drag, and to assess the variation in orbital parameters, we employed two different approaches, and afterward we compared their respective outcomes. The two approaches are:

- *Cartesian Coordinates* propagation: consists in numerically integrating the equation of motion, together with the models for the perturbation assigned. The differential equation to be numerically integrated is:

$$\frac{d^2\mathbf{r}}{dt^2} = -\frac{\mu}{r^3} \mathbf{r} + \sum \mathbf{a}_p \quad (2.11)$$

where \mathbf{a}_p is the vector of the perturbing accelerations.

- *Gauss Planetary Equations*: it's a set of differential equation which, given the six orbital elements $a, e, i, \Omega, \omega, \theta$ at time t_0 and the perturbing acceleration vector \mathbf{a}_p , once numerically integrated for a

well-defined timespan gives us the osculating orbital elements, and afterward the state vector at subsequent times. It's important to highlight also they depends on the reference frame used for the perturbing acceleration. In particular, we have considered two different ref. frame:

- **TNH** (Tangential – Normal – Out-of-Plane) $\xrightarrow{\text{yields}} \mathbf{a}_p^{tnh} = [\hat{\mathbf{t}} \ \hat{\mathbf{n}} \ \hat{\mathbf{h}}] \mathbf{a}_p^{\text{cart}}$
where $[\hat{\mathbf{t}} \ \hat{\mathbf{n}} \ \hat{\mathbf{h}}]$ is the rotation matrix between Cartesian and TNH reference frame.
- **RSW** (Radial – Transversal – Out-of-Plane) $\xrightarrow{\text{yields}} \mathbf{a}_p^{rsw} = [\hat{\mathbf{r}} \ \hat{\mathbf{s}} \ \hat{\mathbf{w}}] \mathbf{a}_p^{\text{cart}}$
where $[\hat{\mathbf{r}} \ \hat{\mathbf{s}} \ \hat{\mathbf{w}}]$ is the rotation matrix between Cartesian and RSW reference frame.

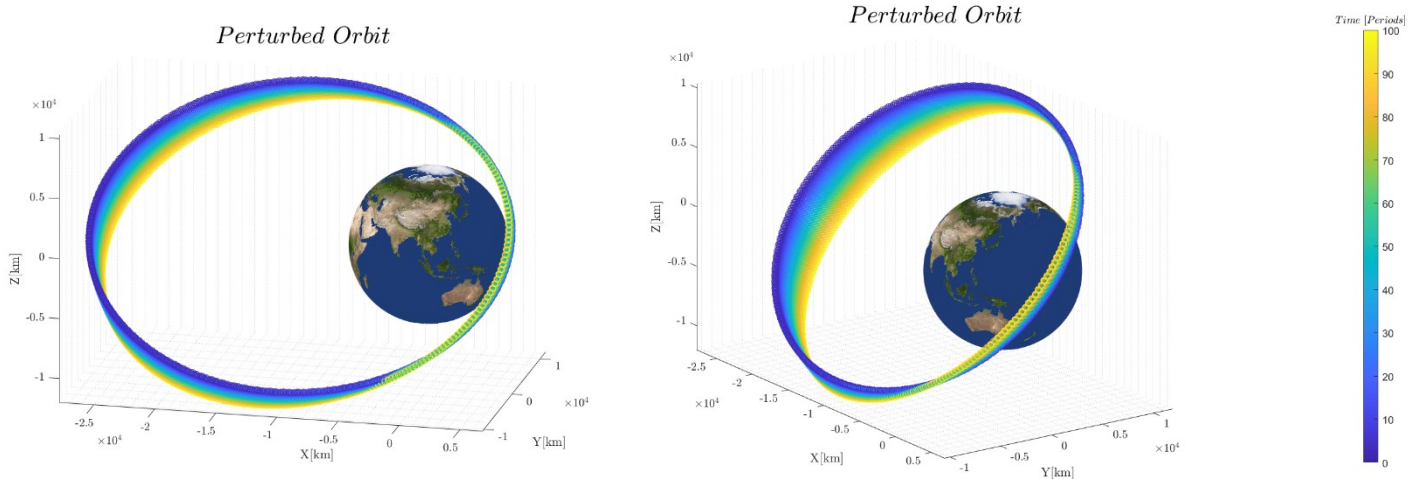


Figure 2.7: Perturbed Orbit over 100 periods

Looking at the figure above, it's clearly possible to notice the effects of J_2 perturbation on Ω and ω and of atmospheric drag which reduces the semimajor axis and the eccentricity.

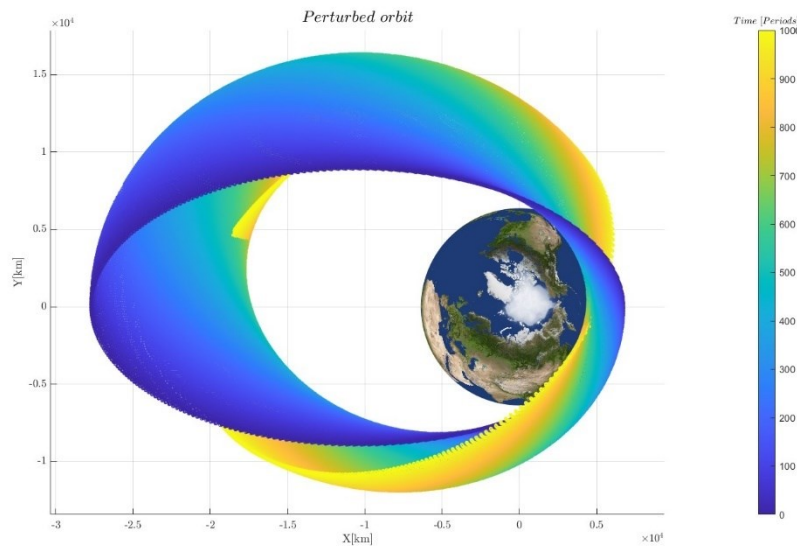


Figure 2.8: Perturbed Orbit over 1000 periods

Given the relatively minor impact on the semi-major axis a and on the eccentricity e compared to other effects on other orbital parameters due to the atmospheric drag, the decision made was to perturb the orbit over a substantial number of periods—specifically, 1000. As depicted Figure 2.8, an examination of the atmospheric drag effects causes a gradual reduction on the semi-major axis, ultimately reaching a point where the pericentre radius falls below the minimum acceptable threshold.

L'orbita, il pericentro NON CAMBIA, il l'apocentro che si avvicina riducendo ₁₂ a e e Cambierà solo una volta raggiunta la cui orbita circolare,

da cui poi si innesca una traiettoria a spirale

2.4 Model Comparison: Analysing Results

Since the orbital perturbations affect the orbital elements in different timescales, filtering the trend of orbital parameters is crucial for a correct understanding of the results obtained from numerical propagation. Furthermore, it allows for assessing the secular evolution of orbital parameters due to perturbations.

The filtering has been performed using a low-pass filter, which removes frequencies (or periods) higher than a given threshold, the cut-off period. The low-pass filter has been designed through the *Matlab function 'movmean'*. Since the considered perturbations, J_2 effect and Atmospheric Drag, have a periodic effect, meaning they repeat at each orbit period, we selected as cut-off period one single orbital period. We then considered the evolution of orbital parameters over 100 periods.

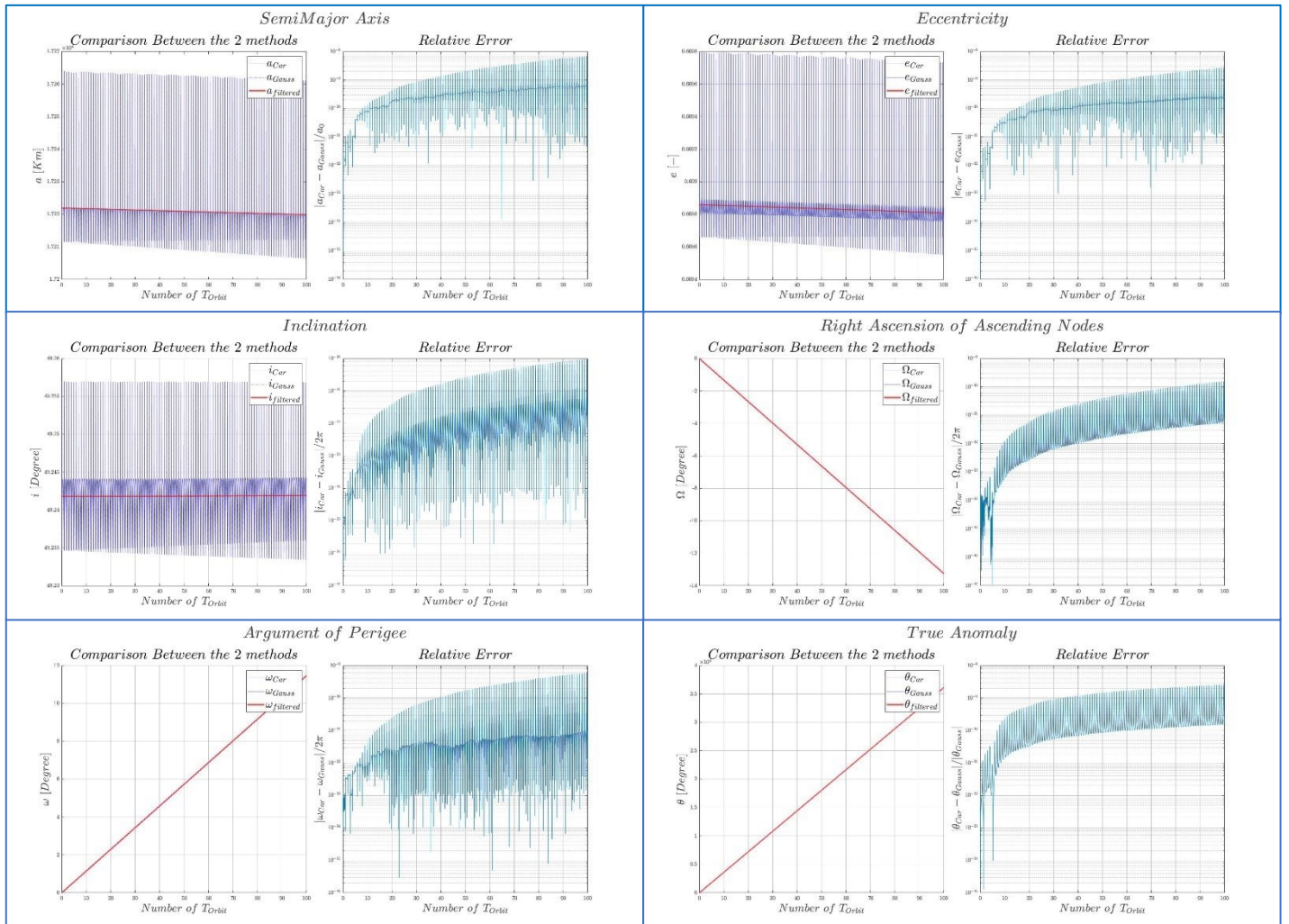


Figure 2.9: On the left plot for each orbital parameter, we have the comparison between the two approaches adopted, and the filtered value in red. On the right, otherwise, there is the relative error between the outcomes of the two methods.

As we can see, the relative error between the orbital parameters calculated with the two different approaches mentioned above is very small, approximately in the range of 10^{-10} . The main difference between the two methods implemented concerns the computational time.

Table 2.2: Computational Time in seconds after 100 periods

Gauss [s]	Cartesian [s]
1.628831	1.309231

The tabulated data clearly indicates a marginal advantage in computational speed for Cartesian coordinates propagation over Gauss planetary equations.

A deeper analysis of this observation reveals that both methods adeptly handle the J2 perturbation effect by leveraging an efficient analytical model for approximation. However, the disparity in performance becomes more pronounced when considering the drag perturbation effect. This particular influence relies on the instantaneous velocity vector, a parameter readily available in the Cartesian method as it is inherently computed. In contrast, the Gauss method necessitates an additional computational step (employing the *kep2car* function) to derive the velocity vector. This supplementary operation, particularly impactful over an extended temporal horizon, contributes to a slightly prolonged overall computational time for the Gauss method.

Another observation we can make by examining the above-mentioned graphs concerns the influence of perturbations on our orbit. The effect of J2 is clear, leading to the regression of the nodal line and, correspondingly, the progression of the argument of perigee and the true anomaly. At the same time, the decrease of semi-major axis and eccentricity is related to Atmospheric Drag. Their variation is minimal can primarily be ascribed to the orbit's elevated values of eccentricity and semi-major axis. Consequently, the duration during which the satellite resides in orbit below 1000 km altitude, where drag becomes non-negligible, is exceedingly brief, in fact $\Delta t = 1009.36$ s which consists in the 4.5% of the orbit period. In conclusion, the inclination remains constant, as none of the perturbations taken into account affects the inclination.

2.5 Model Evaluation

To assess the accuracy of our model, we compared the results obtained with our model against the ephemerides of an authentic celestial object, whose orbit lies in the same orbital region as ours. The selected celestial object is the Debris BREEZE-M DEB (TANK) (NORAD ID: 38344), which is a Russian liquid-propellant rocket orbit insertion upper stage, launched from Baikonur Cosmodrome, Kazakhstan, on May 17th, 2012. We downloaded the ephemerides for a time span of 10 days, starting from November 14th, 2023. The Keplerian elements of its orbit are:

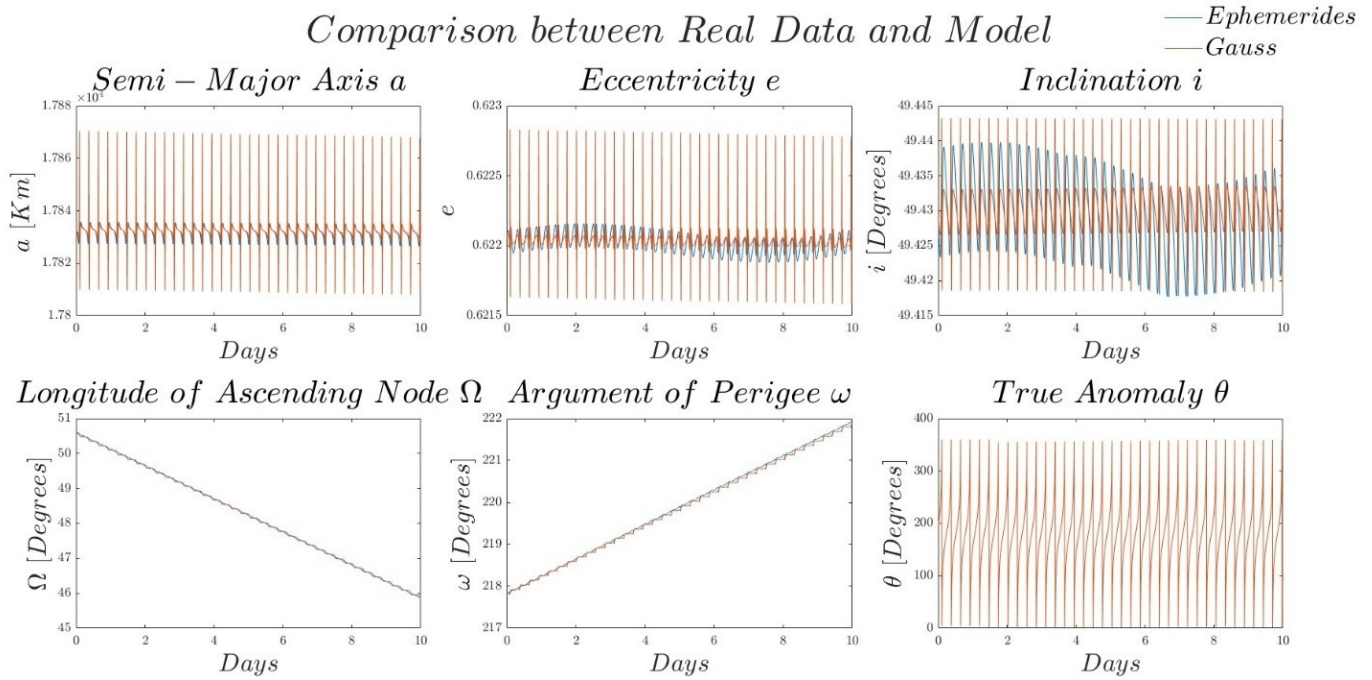
Table 2.3: Keplerian Elements on November 14th, 2023

a [km]	e [-]	i [deg]	Ω [deg]	ω [deg]	θ [deg]	r_p [Km]
17833	0.6221	49.429	50.604	217.812	194.12	363.9

The choice of this celestial object is closely related to the perturbations affecting our original orbit. Indeed, all the parameters on which J_2 effect and Atmospheric Drag depend (a, e, i, r_p) are very close to those of the assigned orbit, while the other parameters are not required to validate our model as they don't affect our perturbations.

The adopted approach involves propagating the orbit of the selected object with our model, using as initial conditions the orbital elements of the selected object at the selected initial time, and then comparing the obtained results with those derived from downloaded ephemerides.

Figure 2.10: Comparison between real data from Ephemerides and the outcomes of our model



As can be observed, the difference between the results is very small, indicative of the effectiveness of the implemented model in assessing the variation of orbital parameters due to J_2 and Atmospheric Drag.

3. References

- [1] Space-Track: <https://www.space-track.org>
- [2] NASA/JPL's HORIZONS: <https://ssd.jpl.nasa.gov/horizons/app.html>
- [3] H. Curtis, 'Orbital Mechanics for Engineering Students'
- [4] D. Vallado, 'Fundamentals of Astrodynamics and Applications'
- [5] Lecture slides of 'Orbital Mechanics' course A.Y. 2023-2024